Dalton Transactions

RSC Publishing

COMMUNICATION

View Article Online
View Journal | View Issue

Cite this: *Dalton Trans.*, 2013, **42**, 885

Received 3rd September 2012,
Accepted 9th November 2012

DOI: 10.1039/c2dt32024j

www.rsc.org/dalton

Homogeneous synthesis of SiO_2@TiO_2 nanocomposites with controllable shell thickness and their enhanced photocatalytic activity†

Yong Yu, Ming-Zhen Zhang, Jun Chen and Yuan-Di Zhao*

Here we report the use of sulfuric acid as a catalyst for the facile and homogeneous synthesis of core–shell SiO_2@TiO_2 nanocomposites using simple apparatus, under ambient pressure and temperature. The resultant SiO_2@TiO_2 exhibits an ideal core–shell structure with uniform nanoscale TiO_2 coverage. The shell thickness of SiO_2@TiO_2 can be conveniently tuned through adjustment of the esterification reaction parameters. Moreover, SiO_2@TiO_2 shows improved catalytic activity in the photodegradation of methyl orange.

Titanium dioxide (TiO_2) has received much attention in areas ranging from electrode to solar energy conversion due to its excellent properties,[1–3] like non-toxicity, chemical stability, and photoactivity.[4–6] In particular, the photo-generated electron–hole pairs in TiO_2 may effectively catalyze a light-induced redox process, which indicates the great potential applications in environmental protection. However, currently available bulk TiO_2 still suffers from some problems in practical utilization. For example, a slurry reactor is the most commonly used operation mode for the treatment of pollutants in water.[7] Nevertheless, on one hand, the commonly used capping ligands for maintaining colloidal stability in colloidal routes often occupy the active sites of TiO_2. On the other hand, these nanoscale TiO_2 nanoparticles (NPs) usually have a spontaneous aggregation in the reaction system, which decreases the effective surface area of TiO_2 and results in a decay of photocatalytic activity.[8] Moreover, a hard process is required to separate ultrafine NPs from aqueous or gaseous pollutants while reclaiming the photocatalysts.

In the past few decades, many efforts have been devoted to the enhancement of immobility/separability of TiO_2.[9–11] In fact, lots of outstanding applications depend not only on the properties of TiO_2 itself but also on the modifications of the TiO_2 material host. Therefore, as one of the effective strategies with unique advantages, such as core/shell processability, capability of self-assembly, and electronic/catalytic reactivities, the synthesis of composites provides the possibility of solving the above-mentioned issues, which couples TiO_2 with other functional materials and thus brings unprecedented novel properties or substantially improves the original properties of the bulk TiO_2.[12,13] Such advantages have stimulated intensive efforts to the screening test on a broad range of materials, like Fe_3O_4, CNTs and SnO_2.[14–16] Among various functional materials, owing to the excellent properties of silica (SiO_2), such as low cost, thermal stability, good absorption, and chemical inertness in solution, fabrication of SiO_2 into TiO_2-based composite attracts tremendous attention, which shows the better catalytic properties than that of bulk TiO_2.[17,18] For example, Kim *et al.* reported the synthesis of nitrogen-doped SiO_2/TiO_2 core/shell NPs through sol–gel reaction.[19] Ding *et al.* used chemical vapor deposition (CVD) process to prepare TiO_2 supported on porous solids.[20] Despite these advantages, currently available synthetic methods are restricted to some limitations. Hydrothermal process asks for complex equipment and high pressure.[21] Functional materials with flat surface or small size (<100 nm) are strict prerequisites for the utilization of CVD or microemulsion. Liquid phase deposition (LPD) suffers from rapid and uncontrolled hydrolysis of TiO_2 precursor. Therefore, the preparation of TiO_2-based composite with ideal hybrid structure through a facile and controllable process still remains a challenge.[22]

To circumvent these difficulties, we report a facile method to prepare core–shell SiO_2@TiO_2 composites with a tunable synthetic process. As a major deviation from the method most commonly used in the literature, the reaction system produces H_2O by itself without extra addition, opening the door to the mild and homogeneous hydrolysis of TiO_2 precursor. Moreover, this technique is carried out in environmentally benign conditions with simple apparatus, ambient pressure and temperature.

Britton Chance Center for Biomedical Photonics, Wuhan National Laboratory for Optoelectronics, Department of Biomedical Engineering, Huazhong University of Science and Technology, Wuhan, HuBei 430074, P.R. China.
E-mail: zydi@mail.hust.edu.cn; Fax: +86-27-87792202; Tel: +86-27-87792235

† Electronic supplementary information (ESI) available: Experimental details and TEM/SEM images. See DOI: 10.1039/c2dt32024j

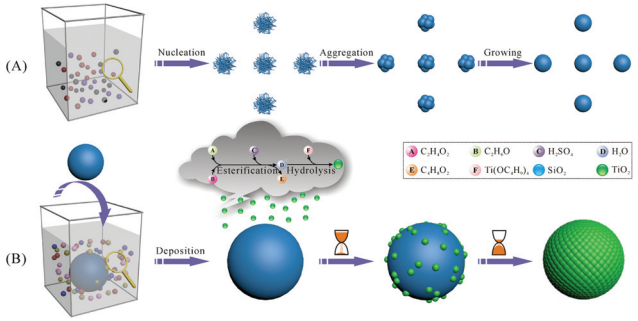

Scheme 1 Schematic illustration of the synthetic procedure for SiO_2 NPs (A) and SiO_2@TiO_2 composite (B).

For the synthetic process of SiO_2@TiO_2 composite, SiO_2 NPs was firstly prepared by dilute ammonia in a mixture of ethanol and tetraethoxysilane (TEOS), according to the previously published procedure.[23] After the process of nucleation and aggregation (Scheme 1A), transmission electron microscopy (TEM) image (Fig. S1, ESI†) shows the resultant SiO_2 has a clean surface and spherical shape. Moreover, these NPs exhibit a narrow size distribution with a diameter of about 450 nm (Fig. S2, ESI†). Further X-ray diffraction (XRD) confirms the characteristic featureless band of SiO_2 (Fig. S3, ESI†). Then, SiO_2 was added into a tetrabutyl titanate (TBT) solution which was prepared by mixing TBT, sulfuric acid, and acetic acid in ethanol. After that, acetic acid and ethanol were catalyzed by sulfuric acid in esterification and formed H_2O, which triggered the hydrolysis of TBT and led to TiO_2 being deposited on the SiO_2 surface (Scheme 1B). Owing to the large number of functional groups on the SiO_2 surface (–OH), which may act as nucleation sites for the deposited clusters and result in a homogeneous distribution of TiO_2 NPs.[19] During the long-drawn out process, the increasing $Ti(OH)_4$ enriches on the SiO_2 surface and gradually aggregates with each other forming a dense covering. Importantly, the mild and homogeneous esterification acts as a valve to slow-release H_2O, which eases the hydrolysis of the TiO_2 precursor, avoiding the inevitable inhomogeneous aggregation of TiO_2, and favouring uniform TiO_2 covering.

The synthesized sample with its core–shell structure was firstly examined by TEM. Fig. 1a shows uniform slightly lighter TiO_2 NPs outside the darker centers of SiO_2. These TiO_2 NPs have near spherical shapes and a narrow size distribution, which verifies the formation of a core–shell structure and indicates the present method is a mild and homogeneous hydrolysis of TiO_2 precursor. A further closer examination of these NPs reveals diameters of about 10 nm (inset of Fig. 1a). A high resolution TEM (HR-TEM) image of SiO_2@TiO_2 is further demonstrated in Fig. 1b, which shows well the crystallization of TiO_2 NPs on the SiO_2 surface. The higher magnification HR-TEM image suggests a distinct lattice spacing of 0.35 nm (Fig. 1c) of TiO_2, which can be indexed to the (101) facet of the anatase crystal structure.[21] The inset of Fig. 1c shows the selected area electron diffraction (SAED) pattern of SiO_2@TiO_2, which exhibits an anatase phase in SiO_2@TiO_2 and is similar

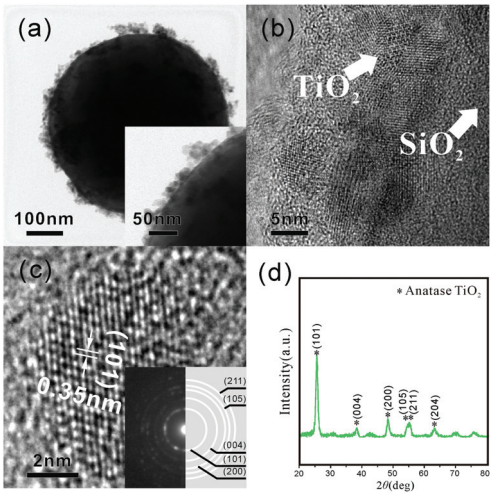

Fig. 1 (a) Low and high (inset) magnification TEM images of SiO_2@TiO_2. Low (b) and high (c) magnification HR-TEM images of SiO_2@TiO_2 (inset shows the corresponding SEAD pattern). (d) XRD pattern of SiO_2@TiO_2.

to the results of HR-TEM. Subsequent crystallization of the outer TiO_2 layer has also been confirmed by the X-ray powder diffraction (XRD) pattern in Fig. 1d. Compared with the featureless XRD pattern of SiO_2 (Fig. S3, ESI†), SiO_2@TiO_2 calcined at 500 °C exhibits clear diffraction peaks at 2θ = 25.2, 38.5, 48.3, 54.1/55.7 (overlapped) and 62.8°, which can be readily indexed to (101), (004), (200), (105/211) and (204) reflections of anatase TiO_2.[22] The energy-dispersive X-ray (EDX) spectrum of SiO_2@TiO_2 (Fig. S4, ESI†) reveals the existence of Si and Ti elements. Fig. S5† shows the SEM image of SiO_2@TiO_2, which demonstrates the distribution of TiO_2 NPs on the SiO_2 surface clearly (ESI†). Nitrogen adsorption and desorption isotherms for SiO_2 and SiO_2@TiO_2 are shown in Fig. S6a (ESI†). It can be seen from the isotherm that SiO_2 has a low adsorbed volume, which results in the dense and non-porous structure of SiO_2. After preparation of the composite, SiO_2@TiO_2 showed increased adsorbed volumes. Importantly, SiO_2@TiO_2 has a type IV isotherm with a hysteresis loop, indicating the presence of a mesoporous structure. The inset of Fig. S6a† shows the pore size distributions of SiO_2 and SiO_2@TiO_2, which suggests SiO_2 has no pore size distributions and SiO_2@TiO_2 has a pore diameter about 4–5 nm. Moreover, the textural properties of SiO_2 and SiO_2@TiO_2 are shown in Fig. S6b (ESI†).

Surface scanning electron microscopy (SEM) images of Fig. 2 show the morphology evolution of SiO_2@TiO_2 prepared from reaction times of 0 h, 6 h, 12 h, and 24 h, respectively. It can be seen that prior to the formation of composite (0 h), SiO_2 NPs shows a smooth and clean surface. When the reaction time is prolonged to 6 h, SiO_2@TiO_2 exhibits a scattered and thin TiO_2 covering on the SiO_2 surface with a thickness of around 20 nm. Along with continued increase in the reaction time, the density of the TiO_2 shell increases gradually. SiO_2@TiO_2 with a reaction time of 12 h (Fig. 2c) shows an obvious textured TiO_2 covering with a thickness of around

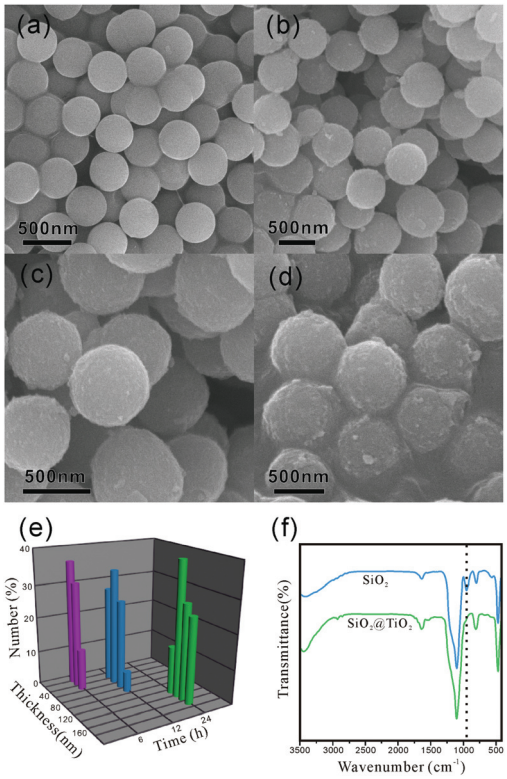

Fig. 2 SEM images of SiO_2@TiO_2 prepared from different reaction times: 0 h (a), 6 h (b), 12 h (c), and 24 h (d). (e) Relationship between the shell thickness of SiO_2@TiO_2 and the reaction time. (e) FT-IR spectrum of SiO_2 and SiO_2@TiO_2.

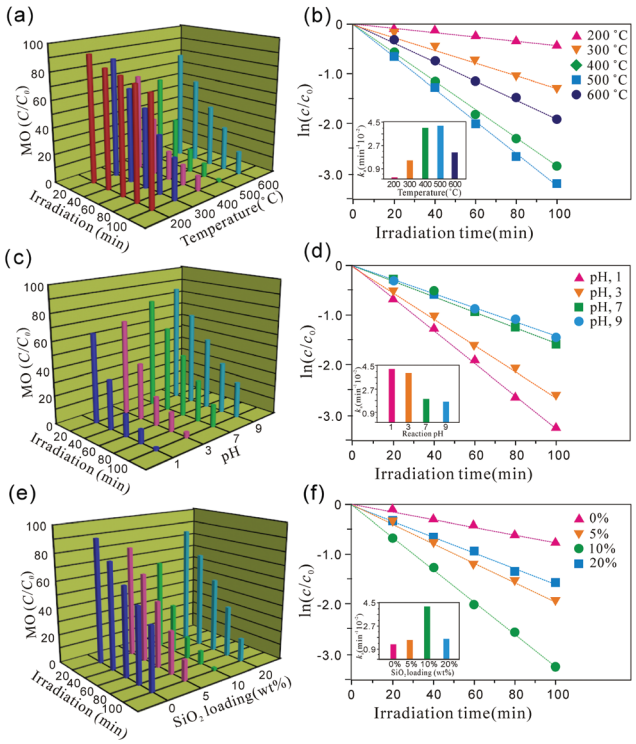

Fig. 3 Evolution of MO concentration *versus* UV irradiation time with different calcination temperature (a), reaction pH (c), and SiO_2 loading (e). Apparent reaction rate constant *versus* UV irradiation time with different calcination temperature (b), reaction pH (d), and SiO_2 loading (f). Pseudo first order constant *versus* different calcination temperature (inset of b), reaction pH (inset of d), and SiO_2 loading (inset of f).

60 nm. When the reaction time is extended to 24 h (Fig. 2d), SiO_2@TiO_2 represents a rougher surface than that of others and the shell thickness is around 140 nm. The shell thickness of SiO_2@TiO_2 under different reaction times is summarized in Fig. 2e by the laser diffraction method, which suggests the shell thickness of the composite can be conveniently tuned through adjustment of the reaction time. Fig. 2f shows the Fourier Transform Infrared Spectroscopy (FT-IR) of SiO_2 and SiO_2@TiO_2. It can be seen that SiO_2 exhibits the obvious absorption bands at 3435 cm^{-1}, 1634 cm^{-1}, 1100 cm^{-1}, and 950 cm^{-1}, which can be readily assigned to the asymmetric or symmetric stretching of OH, H_2O, Si–O–Si, and Si–OH. However, the SiO_2@TiO_2 composite shows the disappearance of characteristic peaks of pure SiO_2 at 950 cm^{-1}. Importantly, the broad peak around 3400 cm^{-1} –OH groups is known as surface hydroxylation for the improvement of photoactivity of TiO_2 through high absorption towards oxygen and reactant molecules.

Photodegradation of methyl orange (MO) is evaluated to demonstrate the improved catalytic activity of TiO_2 through the formation of composite. The UV-vis absorption spectra of MO with various catalysts are shown in Fig. S7–S10 (ESI†). Fig. 3a, 3c and 3e show the influence of calcination temperature, reaction pH, and SiO_2 loading on the degradation of SiO_2@TiO_2. In order to compare the reaction kinetics and explore the optimal parameters, we re-plotted the results of different conditions *versus* UV irradiation time to the first-order reaction rate equation. Fig. 3b, 3d and 3f show the linear relationship represented by the $\ln(C/C_0)$ *versus* reaction time for different calcination temperatures and reaction pH. As all these plots match the first-order reaction kinetics well, the apparent reaction rate constant (k) can be calculated from the rate equation $\ln(C/C_0) = -kt$. It can be seen from the inset of Fig. 3b that SiO_2@TiO_2 calcined at 200 °C has negligible activity and k value increased as calcination temperature increased from 200 °C to 500 °C. When the calcination temperature reached 500 °C, SiO_2@TiO_2 shows the highest k value among the control catalysts (0.041 min^{-1}), which removes more than 90% MO within 100 min. However, the k value decreased as calcination temperature increased to 600 °C (0.023 min^{-1}), which is around two times less than that of SiO_2@TiO_2 calcined at 500 °C. Inset of Fig. 3d shows the MO degradation under various pH values. It can be seen that an acidic pH value is favorable for the degradation of MO and SiO_2@TiO_2 with the reaction pH of 1 showing the highest k value. TiO_2 NPs are the main active centers for MO photodegradation, and the amount of TiO_2 will obviously influence the SiO_2@TiO_2 catalytic activity. Therefore, the effect of SiO_2 loading of SiO_2@TiO_2 on degradation is shown in Fig. 3f. It can be seen from the inset of Fig. 3f that the catalytic activity of SiO_2@TiO_2 increases with increased SiO_2 loading. The k

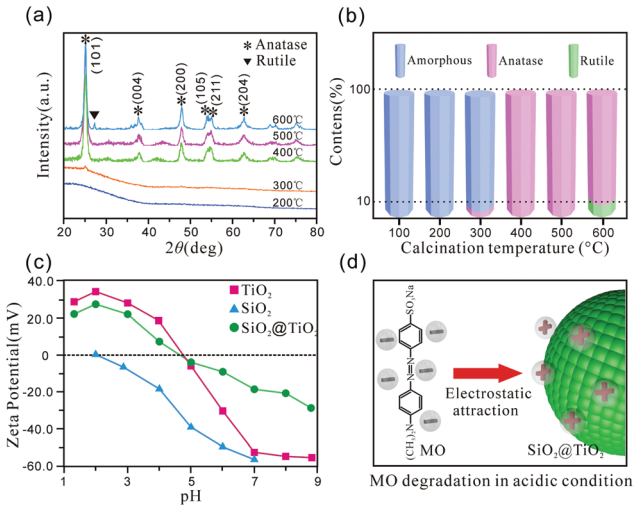

Fig. 4 XRD patterns (a) and phase revolution (b) of $SiO_2@TiO_2$ with different calcination temperatures (200–600 °C). (c) Effect of pH on zeta potential of SiO_2, TiO_2, and $SiO_2@TiO_2$. (d) Schematic illustration for the interaction between MO and $SiO_2@TiO_2$ in acidic conditions.

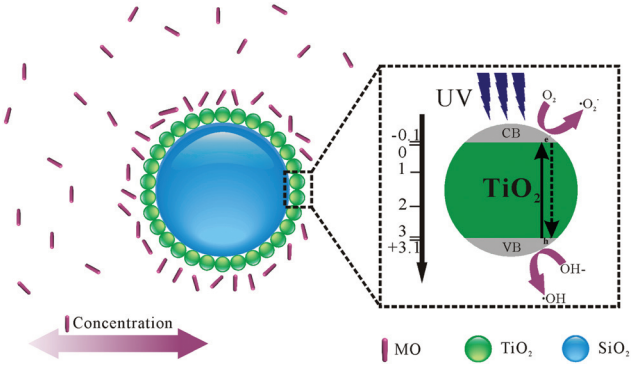

Scheme 2 Schematic illustration for the degradation mechanism of MO with $SiO_2@TiO_2$ under UV light.

value of $SiO_2@TiO_2$ with a SiO_2 loading of 10 wt% is 0.041 min^{-1}, which is nearly 3 times that of bulk TiO_2 alone, which results from the appropriate ratio (10%) of SiO_2 having good absorption towards MO and enhancing the enrichment of MO around TiO_2 as well as the catalytic activity. However, above a certain level (20%), MO degradation efficiency is decreased with increased SiO_2 loading, which can be as a result of excess SiO_2 loading deceasing the amount of active TiO_2 catalyst in the reaction.

The influence of calcination temperature and reaction pH on degradation can contribute to the phase transformation of TiO_2 from active anatase to inactive rutile at higher calcination temperature (600 °C) and electrostatic interaction between MO and $SiO_2@TiO_2$. Fig. 4a shows the XRD patterns of $SiO_2@TiO_2$ calcined at different temperatures. In addition to the featureless XRD pattern of SiO_2, $SiO_2@TiO_2$ calcined at 200 °C has no diffraction peaks from TiO_2, which suggests TiO_2 under present temperatures is still amorphous and causes the inactive phase of TiO_2 has little photoactivity. When the temperature increases to 300 °C, a weak diffraction peak assigned to anatase at $2\theta = 25.2°$ is observed, which suggests the beginning of phase transformation from amorphous to anatase. The appearance of the active anatase TiO_2 leads to the relative higher catalytic activity of $SiO_2@TiO_2$ calcined at 300 °C compared with that of the low temperature (200 °C). When the temperature reaches 400–500 °C, the clear diffraction peaks at 2θ = 25.2, 38.5, 48.3, 54.1/55.7 (overlapped) and 62.8° can be readily indexed to (101), (004), (200), (105/211) and (204) reflections of anatase TiO_2.[24] Owing to the enhanced crystallinity of the active anatase phase, $SiO_2@TiO_2$ calcined at 500 °C has the highest catalytic activity. When the temperature reaches 600 °C, the appearance of weak diffraction peaks of rutile at 2θ = 27.4° indicates transformation from anatase to rutile has occurred. The amount of rutile TiO_2 can be quantified by comparing the integrated intensities of anatase (101) ($A_{anatase}$) and rutile (110) reflections (A_{rutile}).[25]

Based on the equation, the content of rutile TiO_2 is calculated to be 10.28% for $SiO_2@TiO_2$ at 600 °C (Fig. 4b), which results in the decrease of catalytic activity of $SiO_2@TiO_2$. Fig. 4c shows the effect of pH on the zeta potential of SiO_2, TiO_2, and $SiO_2@TiO_2$. Due to the surface OH groups, the zeta potential of each sample increases as the pH of the solution decreases. After TiO_2 deposited on the SiO_2 surface, the isoelectric point (IEP) of $SiO_2@TiO_2$ changed from 2.6 of SiO_2 to 4.8, becoming closer to that of pure TiO_2. Therefore, positive $SiO_2@TiO_2$ has am easy absorption of negative MO at low pH through electrostatic attraction (Fig. 4d), which results in the enrichment of MO around TiO_2 as well as the catalytic activity.

Scheme 2 shows the proposed schematic illustration for the degradation of MO under UV light. Owing to the excellent absorption towards reactant molecules, SiO_2 significantly increases the local concentration of MO near the TiO_2 photoactive layer relative to the bulk solution, which results in an intimate and efficient contact between MO and the short-living superoxide radical ion or hydroxyl radicals on the TiO_2 surface. In contrast to $SiO_2@TiO_2$ with the assistance of SiO_2, without a highly adsorbent support, MO must collide with bulk TiO_2 NPs by chance, and remain in contact for the photocatalysis to proceed. If an efficient collision is not achieved, MO will pass back into the solution and can only react further when they collide with bulk TiO_2 NPs again. Therefore, on the one hand, TiO_2 acts as catalytic centers for the generation of photoinduced radicals, on the other hand, SiO_2 provides plentiful adsorption sites in the vicinity of the TiO_2 catalytic centers. The synergistic effect leads to higher photoactivity of $SiO_2@TiO_2$ than TiO_2 alone.[26–29]

In summary, a facile process has been used to readily prepare core–shell $SiO_2@TiO_2$ composite consisting of uniform TiO_2 nanoshells. Moreover, the shell thickness of $SiO_2@TiO_2$ can be conveniently tuned through adjustment of the reaction time. Unlike other conventional methods, such as hydrothermal, CVD, and microemulsion, the reaction system itself produces H_2O without the need for extra addition

and is carried out under environmentally benign conditions with simple apparatus, at ambient pressure and temperature. As a representative example of synergistic properties of the formation of the core–shell structure, enhanced photocatalysis under UV light has been demonstrated, which suggests anatase TiO_2, appropriate SiO_2 loading, and low pH is in favour of MO photodegradation. SiO_2 has shows good absorption towards MO and enhances the enrichment of MO around TiO_2 as well as the catalytic activity.

Acknowledgements

This work was supported by the National Key Technology R&D Program (2012BAI23B02), National Natural Science Foundation of China (Grant No. 81071229, 81271616), Specialized Research Fund for the Doctoral Program of Higher Education of China (No. 20100142110002), the Fundamental Research Funds for the Central Universities (HUST, 2012TS016). We also thank Analytical and Testing Center (HUST) for assistance with measurements.

Notes and references

1 A. Fujishima, X. T. Zhang and D. A. Tryk, *Surf. Sci. Rep.*, 2008, **63**, 515.
2 K. Sayama, K. Hara, N. Mori, M. Satsuki, S. Suga, S. Tsukagoshi, Y. Abe, H. Sugihara and H. Arakawa, *Chem. Commun.*, 2000, 1173.
3 Y. Zhou, F. Krumeich, A. Heel and G. R. Patzke, *Dalton Trans.*, 2010, **39**, 6043.
4 Y. B. Liu, J. H. Li, B. X. Zhou, X. J. Li, H. C. Chen, Q. P. Chen, Z. S. Wang, L. Li, J. L. Wang and W. M. Cai, *Water Res.*, 2011, **45**, 3991.
5 U. Diebold, *Surf. Sci. Rep.*, 2003, **48**, 53.
6 X. Chen and S. S. Mao, *Chem. Rev.*, 2007, **107**, 2891.
7 B. H. Wu, C. Y. Guo, N. F. Zheng, Z. X. Xie and G. D. Stucky, *J. Am. Chem. Soc.*, 2008, **130**, 17563.
8 H. G. Yang, C. H. Sun, S. Z. Qiao, J. Zou, G. Liu, S. C. Smith, H. M. Cheng and G. Q. Lu, *Nature*, 2008, **453**, 638.
9 Y. Q. Wang, S. G. Chen, X. H. Tang, O. Palchik, A. Zaban, Y. Koltypin and A. Gedanken, *J. Mater. Chem.*, 2001, **11**, 521.
10 E. Stathatos, P. Lianos, S. M. Zakeeruddin, P. Liska and M. Gratzel, *Chem. Mater.*, 2003, **15**, 1825.
11 Z. P. Liu, P. Hu and A. Alavi, *J. Am. Chem. Soc.*, 2002, **124**, 14770.
12 H. S. Shin, Y. S. Jang, Y. Lee, Y. Jung, S. B. Kim and H. C. Choi, *Adv. Mater.*, 2007, **19**, 2873.
13 F. Caruso, *Adv. Mater.*, 2001, **13**, 1577.
14 C. L. Zhu, M. L. Zhang, Y. J. Qiao, G. Xiao, F. Zhang and Y. J. Chen, *J. Phys. Chem. C*, 2010, **114**, 16229.
15 A. Kongkanand, R. M. Dominguez and P. V. Kamat, *Nano Lett.*, 2007, **7**, 676.
16 J. Qian, P. Liu, Y. Xiao, Y. Jiang, Y. Cao, X. Ai and H. Yang, *Adv. Mater.*, 2009, **21**, 3663.
17 S. H. Zhan, D. R. Chen, X. L. Jiao and Y. Song, *Chem. Commun.*, 2007, 2043.
18 J. L. Zhang, Z. M. Liu, B. X. Han, Z. H. Li, G. Y. Yang, J. C. Li and J. Chen, *J. Supercrit. Fluids*, 2006, **36**, 194.
19 C. Kim, M. Choi and J. Jang, *Catal. Commun.*, 2010, **11**, 378.
20 Z. Ding, X. J. Hu, P. L. Yue, G. Q. Lu and P. F. Greenfield, *Catal. Today*, 2001, **68**, 173.
21 Z. Y. Wu, Y. F. Tao, Z. Lin, L. Liu, X. X. Fan and Y. Wang, *J. Phys. Chem. C*, 2009, **113**, 20335.
22 K. Koumoto, S. Seo, T. Sugiyama, W. S. Seo and W. J. Dressick, *Chem. Mater.*, 1999, **11**, 2305.
23 J. B. Joo, Q. Zhang, M. Dahl, I. Lee, J. Goebl, F. Zaera and Y. D. Yin, *Energy Environ. Sci.*, 2012, **5**, 6321.
24 B. Bonelli, M. Cozzolino, R. Tesser, M. Di Serio, M. Piumetti, E. Garrone and E. Santacesaria, *J. Catal.*, 2007, **246**, 293.
25 H. Z. Zhang and J. F. Banfield, *J. Phys. Chem. B*, 2000, **104**, 3481.
26 H. Wang, M. Yu, C. K. Lin and J. Lin, *J. Colloid Interface Sci.*, 2006, **300**, 176.
27 F. L. Arbeloa, V. M. Martinez, J. B. Prieto and I. L. Arbeloa, *Langmuir*, 2002, **18**, 2658.
28 A. L. Linsebigler, G. Lu and J. T. Yates, *Chem. Rev.*, 1995, **95**, 735.
29 B. Gao, C. Peng, G. Z. Chen and G. L. Puma, *Appl. Catal., B*, 2008, **85**, 17.